Molecular effects on boundary condition in micro/nanoliquid flows

Umberto Ulmanella[1] and Chih-Ming Ho[2]
[1]*Applied Biosystems, Foster City, California 94404, USA*
[2]*Department of Mechanical and Aerospace Engineering, University of California–Los Angeles, Los Angeles, California 90095, USA*

(Received 9 January 2008; accepted 25 May 2008; published online 31 October 2008)

We experimentally investigated molecular effects of the slip/no-slip boundary condition of Newtonian liquids in micro- and nanochannels as small as 350 nm. The slip was measurable for channels smaller than approximately 2 μm. The amount of slip is found to be independent of the channel size, but is a function of the shear rate, the type of liquid (polar or nonpolar molecular structure), and the morphology of the solid surface (molecular-level smoothness). © *2008 American Institute of Physics*. [DOI: 10.1063/1.3006031]

I. INTRODUCTION

In the continuum regime of Newtonian fluid flow, the molecular effects are simply represented by the viscosity and the boundary condition. Viscosity is a measure of forces among fluid molecules. Boundary slip/nonslip indicates the interaction between fluid molecule and the surface. The value of the viscosity usually does not change significantly in this regime. However, in the layer of a few fluid molecule thickness above the solid surface, the viscous stresses can be very different from what was predicted from the conventional viscosity definition because the force exerted on fluid molecules by the potential of the molecules in the solid becomes appreciable.[1,2] The modification of the nonslip boundary condition depends on whether the fluid is a gas or a liquid. For gas flows, the molecules are separated far apart and the intermolecular interactions are therefore very simple compared with a liquid. With no interaction force except collisions, the surface slip of gas flow is a function of Knudsen number. Due to the close proximities, the interactions among liquid molecules are stronger. In addition, under the same physical conditions (i.e., temperature and pressure) the structure of a liquid molecule can be much more intricate than the usually smaller gas molecules. The breakdown of the nonslip boundary condition in liquid flow is a rich phenomenon which has received increasing attention in the last few years. Although a growing number of numerical and experimental studies have been performed to date, different works present inconsistent findings and a clear understanding on the causes at the root of this phenomenon is still needed.[3,4] One of the reasons is the difficulty in achieving the necessary experimental sensitivity and accuracy at the unusually small length scales that compete to this phenomenon. Another reason is the difficulty in comparing results obtained by dissimilar experimental methodologies, i.e., the capillary rheometer, the surface force apparatus, the atomic force microscope (AFM), the crystal resonator, and the direct imaging of the flow through photobleaching or μPIV. The concept that effective slip can occur at a liquid-solid interface is generally accepted, with its main contributors being the wettability and the roughness of the boundary, although results obtained with different techniques, or even with the same technique, may show opposite trends. For example, experiments with the surface force apparatus and the AFM show that slip of water or aqueous solutions can be both shear dependent,[5,6] or independent,[7,8] while the findings from pressure driven flow or Couette flow mostly agree on the constant slip length model,[9–12] with a more recent exception.[13]

Evidence of slip on hydrophilic surfaces was found with the surface force apparatus,[9,12] and a systematic investigation on surface roughness in a Couette flow determined the contribution of different aspects of surface morphology to slip.[14] According to a different set of studies with the surface force apparatus, slip was found only on nonwetting surfaces.[7,8]

In microchannel flow, slip of a highly polar liquid is found, both in numerical simulations and experiments, to occur on smooth hydrophobic walls,[8–11,13–18] and limited evidence of slip has been reported on hydrophilic surfaces.[18,19]

In this work, we have investigated how the liquid-boundary strength of interaction and boundary morphology affect the slip of liquids in pressure driven flows of simple liquids. Experiments with pure liquids of different polar natures, isopropanol and *n*-hexadecane, were performed for this purpose in micro- and nanochannels between 350 nm and 5 μm in depth with hydrophilic (wetting) walls of different surface roughnesses.[20]

II. EXPERIMENTAL APPARATUS

A rheometric apparatus (Fig. 1) was devised to perform the tests with different liquids in channels with depth in the micron and submicron ranges.

Microfluidic chips containing the channels for the study were fabricated by anodically bonding a 5 mm thick piece of Borofloat glass to a 450 μm thick silicon substrate (Fig. 2). The general layout of the chips consists of a test section channel and of an upstream filtering section constituted by hundreds of channels arranged in parallel and with depth between three and four times less than the test section. The test section is obtained by a two-step HF etching process: a 200+2000 Å thick evaporated chromium-gold mask is in a first time patterned to etch only the test section. After the first etch, the filter channels are opened as well on the mask and

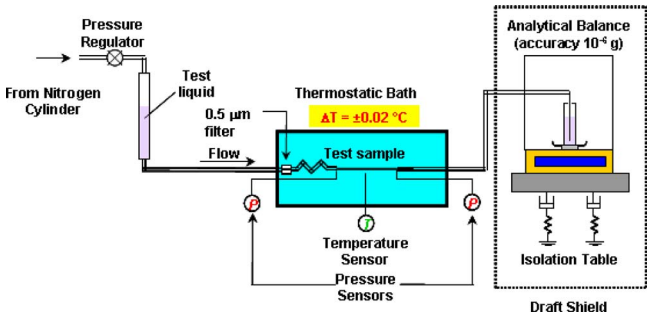

FIG. 1. (Color online) Schematic of experimental apparatus.

the second etching step takes place. The resulting surface roughness of the test section is controlled by the concentration of HF and its depth by the total etching time. On the silicon side, three vias (one fluidic inlet, one fluidic outlet, and one static port) and three deep channel networks (one distribution network from the chip inlet to the filter channels inlets, one manifold between the filter channels outlets and the test section inlet, and one channel between the test section outlet and the chip outlet) are etched through a similar two-step process with KOH Si etching through an oxide-nitride mask. The original roughness of the wafer is preserved in the test section since it is not subjected to etching. To control the roughness on the silicon side, wafers with different levels of surface quality were used. Before assembly, the areas defining the test sections were characterized with a benchtop Veeco Wyco optical profiler. Channel length, width, depth, and cross-sectional shape were determined with scans in vertical scanning interferometry (VSI) mode, while the average surface roughness of the top and bottom channel walls was determined in phase shifting interferometry (PSI) mode. To run the tests on the glass chips in PSI mode, the pieces were coated with a thin metallic layer to enhance reflectivity. After characterization, the layer was removed by a selective metal etchant. The calibration of the instrument was validated in VSI mode with NIST traceable

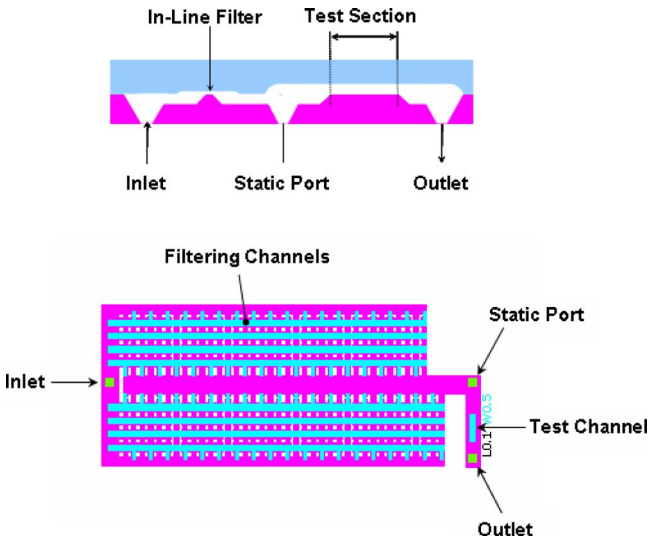

FIG. 2. (Color online) Cross-sectional view and top view of the glass-silicon chips with the integrated filter and the micro- and nanochannels.

calibration standards, while the values of roughness obtained with the profiler on standard specimens of different roughnesses were compared to those obtained by AFM scans. Channel length and width were determined with a 0.1 μm accuracy, while the uncertainty associated with the channel depth was around 2% for the shallowest channels. Glass pieces and silicon chips with comparable levels of surface roughness were eventually matched and, after a 10 min hot piranha clean, bonded together. The dual purpose of the piranha treatment was not only to prepare the surface for bonding but also to guarantee a comparable level of wettability of the surfaces of the two materials.

Several chips with different dimensions of the test section and levels of surface roughness were produced with this process. The depth of the test section varied between 350 nm and 5 μm and the fluidic chips were divided in "smooth" and "rough" depending if the rms surface roughness of the test section was less than 0.5 nm or above 5 nm.

The length of the channels varied between 370 μm and 10 mm and the width ranged between approximately 0.5 and 1 mm. To minimize the influence of entrance and exit losses on the pressure drop between channel inlet and outlet, the length of the channel was chosen so that the ratio of the entrance length, calculated with the no-slip condition, to the total length was less than 1:200 in the worst case scenario. For smaller channels the value was greater by one order of magnitude. To minimize the effect of the sidewalls on the flow, the minimum aspect ratio between width and height of the cross section was 200:1 for the deepest channels, and of the order of 1000:1 for the most shallow ones.

A machined Plexiglass fixture, consisting of two Plexiglass plates holding the microchannel in between and held together by screws was used to hold the test chips. The fluidic ports were aligned to threaded holes in the fixture and high-pressure microfluidic fittings, developed by Lawrence Livermore National Laboratories,[21] were used to connect the fluidic ports and the static pressure port to the outside world. Three special polyetheretherketone (PEEK®) tubes with one molded end were used to interface with the test chips, while standard PEEK tubing and appropriate plastic components (i.e., tees, unions, fittings, adapters, etc.) from Upchurch Scientific were used for the remaining parts of the fluidic path. To thermally isolate the test section from the environmental fluctuations, the fixture was placed in a water bath fluidically connected to an external temperature controlled water circulator. The temperature was held constant by a proportional-integral-derivative controller and the feedback resistance temperature detector probe was placed in close proximity to the test section. The temperature fluctuations of the bath were found to occur at regular intervals, with measured amplitude of ± 0.02 °C and period of the order of tens of minutes. The resulting change in viscosity in the test liquid due to the variation in the local temperature is estimated to be 0.1% or less. The fixture was connected on the upstream side to a pressurized reservoir kept outside of the bath and holding the test liquid. Pressure was applied to the test liquid by a nitrogen cylinder through a high accuracy regulator. A 0.5 μm in-line filter and a long section of coiled tubing were placed between the reservoir and the fixture. The length of

the tubing was experimentally verified to allow the test liquid to reach the bath temperature throughout the whole range of flowrates used in the experiments. Two high accuracy piezoelectric pressure transducers (Micron Instruments) with both linearity and accuracy better than 0.2% were used to measure the pressure at the static port and, through a tee on the liquid path, at the outlet of the chip. The transducers were recalibrated several times between experimental tests with an NIST traceable digital test gauge with accuracy better than 0.1%. The wetted parts of the sensors were coated with Teflon to avoid the dissolution of metallic ions in the test liquid that could affect the electrical neutrality of the test fluids (and/or cause corrosion of the sensors). Due to the low values of Reynolds number in the experiment, the pressure drop between inlet and outlet of the test section is estimated to differ by less than 0.1% from the measured pressure drop Δp. Downstream, the second branch of tubing stemming from the tee at the chip outlet extended outside the water bath to deliver the test liquid to a Mettler-Toledo AT20 analytical balance with repeatability of 4 μg and internal calibration. The instruments in the experimental apparatus (i.e., pressure and temperature meters, water circulator, analytical balance) were connected to a computer through an RS-232 adapter. The test fluid was collected in a glass vial placed on the weighing pan. Several precautions were taken to minimize the mechanical noise affecting the readings of the balance: the balance was placed on an isolation table (Newport) whose top was completely shielded to protect the table and the balance from the air draft due to the room ventilation system. The tubing from the test section was drawn through small holes opened on the shield of the isolation table and on the two shields of the balance and held in place by fixtures anchored to the isolation table. In addition, it carefully routed to minimize the mechanical coupling to the external environment. The vial was prefilled with test fluid. A layer of silicone oil was placed on top of the liquid to prevent its evaporation. Before experimentation, the system was carefully primed to eliminate any bubbles. Additionally, a small amount of fluid was collected in the weighing vial to submerge the end of the delivery tubing a few millimeters below the free surface of liquid. This was done to ensure a smooth and continuous delivery of test fluid to the vial.

III. FLOWRATE DETERMINATION

The basic principle adopted to measure the flowrate was based on the gravimetric measurement of the amount of test liquid collected in the vial placed on the analytical balance. Under steady state conditions, the flowrate of the incompressible test liquid flowing through the test section, $Q_{\text{test section}}$, is equal to the flowrate of liquid Q_{balance} collected in the vial on the scale. This is related to the time rate of change of the weight of test liquid collected in the vial, $\dot{W}_{\text{test liquid}}$, by $Q_{\text{balance}}=\dot{W}_{\text{test liquid}}/\rho g$, where ρ is the density of the test liquid and g the constant of gravity.

The balance of forces acting upon the vial yields

$$W_{\text{balance}} = W_{\text{vial}} + W_{\text{test liquid}} + B_{\text{tube}}, \tag{1}$$

where W_{balance} is the weight measured by the balance, W_{vial} is the weight of the vial, $W_{\text{test liquid}}$ is the weight of test liquid accumulated inside the vial, and B_{tube} the reaction of the buoyant force of the portion of tubing submerged in the collected liquid.

At steady state, the time differential of the above terms yields

$$\dot{W}_{\text{test liquid}} = \dot{W}_{\text{balance}} + \dot{W}_{\text{evaporation}} - \dot{B}_{\text{tube}}, \tag{2}$$

where the dotted variables represent the time rate of change of the forces bearing the same subscript, $\dot{W}_{\text{vial}}=0$ due to fixed mass of the vial, and $\dot{W}_{\text{evaporation}}$ indicates the evaporation rate, in terms of weight, of the fluid collected in the vial. $\dot{B}_{\text{tube}}$ was found to be independent of time and from geometrical arguments estimated to contribute to approximately 1% of $\dot{W}_{\text{test liquid}}$. Additional forces not appearing in Eq. (2) or their time rate of change, such as the force resulting from the momentum loss of the liquid exiting the tubing, the capillary force produced on the vial by the advancing liquid menisci (test liquid/silicone oil and silicone oil/air) contacting it, the viscous forces on the walls of the vial due to the change in level of the collected liquid, are estimated to be either independent of time under steady state conditions, or negligible. $\dot{W}_{\text{balance}}$ and $\dot{W}_{\text{evaporation}}$ are calculated from their average rates of change within a time interval $\Delta t=t_2-t_1$,

$$\dot{W}_{\text{balance}} = \bar{\dot{W}}_{\text{balance}}|_{\Delta t} = \frac{W_{\text{balance},t_2} - W_{\text{balance},t_1}}{t_2 - t_1} = \frac{\Delta W_{\text{balance}}}{\Delta t}, \tag{3}$$

$$\dot{W}_{\text{evaporation}} = \bar{\dot{W}}_{\text{evaporation}}|_{\Delta t} = \frac{W_{\text{evaporation},t_2} - W_{\text{evaporation},t_1}}{t_2 - t_1} = \frac{\Delta W_{\text{evaporation}}}{\Delta t}. \tag{4}$$

To ensure that steady state conditions are actually reached during the measurements for the above equalities to hold, the instantaneous value of the pressure drop Δp across the test section and the rolling value of $\bar{\dot{W}}_{\text{balance}}|_{\Delta t}$ are monitored. Variations in Δp are generally contained within 0.5% of its rms value, while the fluctuations of $\bar{\dot{W}}_{\text{balance}}|_{\Delta t}$ are as large as 20% for $\Delta t=30-60$ s. To ensure that an appropriate sampling time was chosen to reduce the noise level on the measurement on much smaller level, the fixed initial point long-term average was monitored,

$$\dot{W}_{\text{balance},LT} = \frac{W_{\text{balance},t_c} - W_{\text{balance},t_0}}{t_c - t_0}, \tag{5}$$

where t_c is the running experimental time and t_0 is reference time fixed after a steady state in the pressure drop was achieved. With time intervals between 5 and 30 min, the fluctuations on the rms value of $\dot{W}_{\text{balance},LT}$ were reduced to less than the greatest between 1 nl/min and 0.5% (Fig. 3). After this condition was achieved, the acquisition of the data was further extended for a period of two to three times

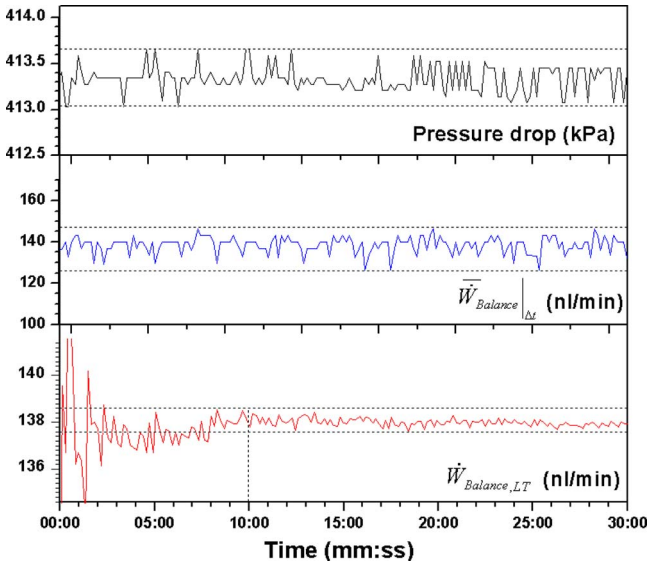

FIG. 3. (Color online) Time trace of pressure drop (top panel), time rate of change of measured weight based on a 30 s time period (middle panel), and long-term rate of change with respect to $t=0$ (bottom panel). Fluctuations in the pressure drop are less than 0.2% rms; those in the rate of change of measured weight are about 20%, while those in the rate of change based on the initial $t=0$ fall below 1 nl/min after about 10 min.

longer. When the raw data were processed, long-term running average mass rate with base period around half of the sampling interval is applied to the entire sampling interval to verify that a steady state had indeed been reached during the sampling time. The average of the running averages was chosen for the mass rate, while the difference between the largest and smallest of their values was chosen as the error, which still was in the order of the greatest between 1 nl/min and 0.5%.

The evaporation rate is estimated using the same process, after fluidically isolating the balance by shutting off a valve located along the fluidic path downstream of the test section. Under such conditions, $\dot{W}_{\text{test fluid}}=0$ and $\dot{W}_{\text{evaporation}}=\dot{W}_{\text{balance}}-\dot{W}_{\text{tube}}$. Based on the same arguments as above, $\dot{W}_{\text{tube}}$ is a fixed and small portion of $\dot{W}_{\text{evaporation}}$, therefore the estimate of the weight rate of evaporation can be obtained from the same process as above and with the same level of accuracy. The evaporation rate is measured before and after each experiment and before and after each data point for which evaporation is expected to be not negligible. In general, $\dot{W}_{\text{evaporation}}$ is on the order of 10 μg/min (corresponding to $\sim$10 nl/min of water) and is found to be substantially constant during the entire duration of one experimental test. With the assumption that the evaporation rate of the layer of oil is not different from when there is flow of test fluid into the vial, $\dot{W}_{\text{evaporation}}$ is equaled to the average of the two values measured before and after a data point. The largest between the uncertainties of the two measurements, increased by the difference between the two measurements, is assigned to the uncertainty of $\dot{W}_{\text{evaporation}}$.

With this method, mass rates of test liquid comparable to the evaporation rate of the silicone oil in the vial could be measured with accuracy as low as a few μg/min.

$Q_{\text{test section}}$ was finally determined from $\dot{W}_{\text{test liquid}}$, under the verified assumption of steady state, where the appropriate values of density of test fluids at the measured temperatures are obtained from the tables.

The described flowrate measurement method was validated within the range of flowrates used in the experiment (10 nl/min–1 ml/min) by measuring the flowrate of test liquids produced by a high accuracy syringe pump (Harvard Apparatus PHD 4400 Hpsi, accuracy of 0.35%). Syringes from 10 μl to 1 ml (Hamilton Gastight) were installed on the syringe pump and connected to the main fluidic path through a tee installed downstream of the test section. With this method, it was also verified that the evaporation rate did not change between static and dynamic conditions.

IV. EXPERIMENTAL PROCEDURE

The experimental range of pressure drop was between 10^5 and 2×10^6 Pa, and $\sim$10 nl/min to $\sim$1 ml/min for the flowrate.

Deionized (DI) water, isopropanol, ethanol, toluene, and *n*-hexadecane were used in the validation of the experimental apparatus with silica capillaries and for the tests with the microchips. DI water was prepared fresh before every experiment by a Barnstead water de-ionizer and had a resistivity of 18.3 MΩ cm. The other test liquids were obtained by Sigma-Aldrich in HPLC grade for isopropanol and ethanol (99.9% purity) and anhydrous grade for toluene and hexadecane (water content of $<$0.003%). All the liquids were used as received and freshly poured before the experiments. After the tests with water and the alcohols, all the components of the fluidic paths were flushed with isopropanol and then purged with a stream of compressed nitrogen for 30 min. Components with a dead end were disconnected at their distal end from the nitrogen tank and purged for an equal amount of time. After the tests with *n*-toluene and hexadecane, all the wetted components were replaced, with the exception of the pressure transducers, which were disconnected and treated with thorough rinses with butanol and ethanol. To prevent contamination of the surfaces of the test section, liquids of the same polar nature (i.e., polar versus nonpolar) were used in each chip. The only exception was the 0.49 μm deep channel, which was first tested with isopropanol and then with hexadecane.

V. VALIDATION OF THE EXPERIMENTAL APPARATUS

Before running experiments on microfluidic chips, the experimental apparatus is validated with DI water, isopropanol, ethanol, toluene, and *n*-hexadecane as test liquids flowing through test sections of polyimide coated fused silica tubing (Polymicro Technologies) with nominal diameters between 6 and 100 μm. Flowrates from tens of nl/min to several ml/min are used in these tests.

The 360 μm outer diameter capillaries were coupled to the 1/16 in. fitting by means of PEEK sleeves placed at the two ends of the capillary. The length of the sections of capillary was chosen to produce values of fluidic resistance comparable to those of the microchips used later so that similar ranges of pressure drop and flowrate were covered in

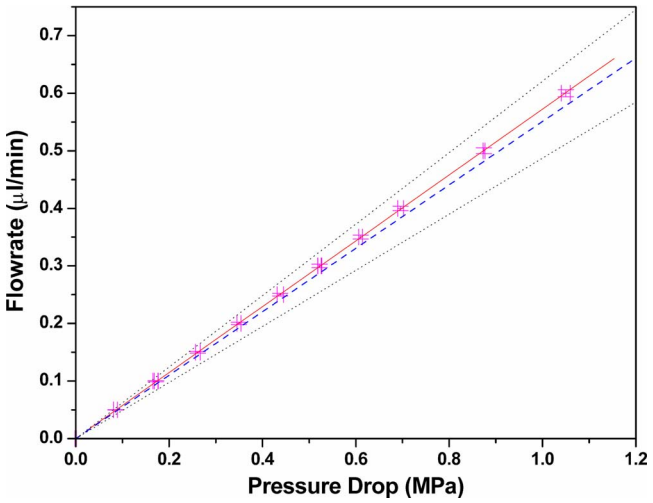

FIG. 4. (Color online) Measured flowrate vs imposed pressure drop for a test with DI water in a 6.6 μm capillary. The solid line represents the linear fit of the experimental data, whose error bars are visible in the graph. The dashed line is the expected pressure drop, while the two dotted lines are the upper and lower uncertainty boundaries.

the process. The length of the capillaries was determined within 0.1 mm by an optical comparator, while the inner diameter was measured by taking scanning electron microscope (SEM) shots of the two ends. NIST traceable calibration graticules were used to verify the calibration of the SEM instrument. The flowrate determined with the analytical balance $Q_{\text{experimental}}$ was compared to the theoretical value $Q_{\text{theoretical}}$ estimated by

$$Q_{\text{theoretical}} = K \cdot \frac{D^4}{\mu \cdot L} \cdot \Delta p, \tag{6}$$

where Δp is the pressure drop produced by the laminar flow of an incompressible fluid of viscosity μ across a rectilinear section of diameter D and length L, and K is a constant related to the shape of the cross section which is equal to $\pi/128$ in the circular case. The slight eccentricity of the test section, always less than 2%, was accounted for by using the hydraulic diameter $D_H = D_1 \cdot D_2/(D_1 + D_2)$ for D and by correcting K accordingly. The validation experiments were tested at various temperatures between 5 and 35 °C, and the value for μ was taken from the tables at the appropriate temperature T or interpolated between known values using Andreade's equation ($\mu = a \cdot e^{b/(T+c)}$), where the coefficients a, b, and c were obtained by least squares fitting of the values available. Different tests are performed and the flow rate is varied both increasing and decreasing it, in order to detect hysteretic effects and repeatability problems in the experimental system.

The measurements showed a linear relationship between measured flowrate and pressure drop in the whole range tested, from 100 μm down to ~6 μm, with values of the R-test for linearity differing from 1 only from the fourth decimal. Furthermore, the difference between measured flowrate and the flowrate predicted with Eq. (6) at the same pressure drop was better than 1% for larger capillaries, less than 3% for the smaller ones (Fig. 4), and always better than the uncertainty of the estimated Q due to the experimental uncertainty on D, L, and Δp.

Great care was taken during the developments of experimental apparatus and procedures. Our experiences indicate that only going through these painstaking processes can lead toward consistent and reliable data.

TABLE I. Summary of experimental conditions and results.

Channel depth	Wall surface	Measured slip length[a] (nm)	
		Isopropanol	*n*-hexadecane
0.35–1.37 μm	Smooth (R_a~0.5 nm)	30	120
	Rough (R_a~8.5 nm)	<5 nm	<5 nm
~5 μm [b]	Smooth (R_a~0.5 nm)	Nondetectable	
	Rough (R_a~8.5 nm)		

[a]At $\dot{\gamma}_w \sim 3 \times 10^5$ s^{-1}.
[b]Similar results were obtained with DI water and ethanol.

VI. RESULTS AND DISCUSSION

After the validation of the experimental apparatus with the circular capillaries, tests with different Newtonian liquids were performed in the micro- and submicron channels described above. All the tests were performed at 20 °C (Table I).

In the absence of slip, the expected flowrate $Q_{\text{Poiseulle}}$ for the laminar flow of an incompressible fluid of viscosity μ through a two-dimensional channel of height H, width W, and length L is given by

$$Q_{\text{Poiseuille}} = \frac{1}{12} \cdot \frac{WH^3}{\mu \cdot L} \cdot \Delta p. \tag{7}$$

If slip is present at the both bounding walls, the total flowrate is increased by $Q_{\text{slip}} = WH \cdot u_{\text{slip}}$, where u_{slip} is the slip at each wall. Due to the similarity between the bounding surfaces, the presence of the same slip velocity is assumed. The slip length β is calculated from the slip length u_{slip} and the wall shear rate $\dot{\gamma}_w$ from

$$\beta = \frac{u_{\text{slip}}}{\dot{\gamma}_w} = \frac{2\mu \cdot L}{WH^2} \cdot \frac{Q}{\Delta p} - \frac{H}{6}. \tag{8}$$

Experimental results obtained on ~5 μm deep smooth (R_a=0.5 nm) channels with all the fluids tested at this size (i.e., DI water, isopropanol, ethanol, and *n*-hexadecane) show a linear dependence (correlation coefficient differing from 1 only from the fourth decimal) between the measured flowrate $Q_{\text{experimental}}$ and the measured pressure drop Δp, indicating a Newtonian behavior of these liquids in channels of this size. In addition, the difference between $Q_{\text{Poiseuille}}$ and $Q_{\text{experimental}}$ falls within the 3% uncertainty interval of these tests (Fig. 5).

The flow rate difference due to slip effect, Q_{slip}, is not appreciable enough to be detected in 5 μm deep channels. This is consistent with the findings obtained from the circular capillaries of similar diameter (6 μm) used for the system validation tests.

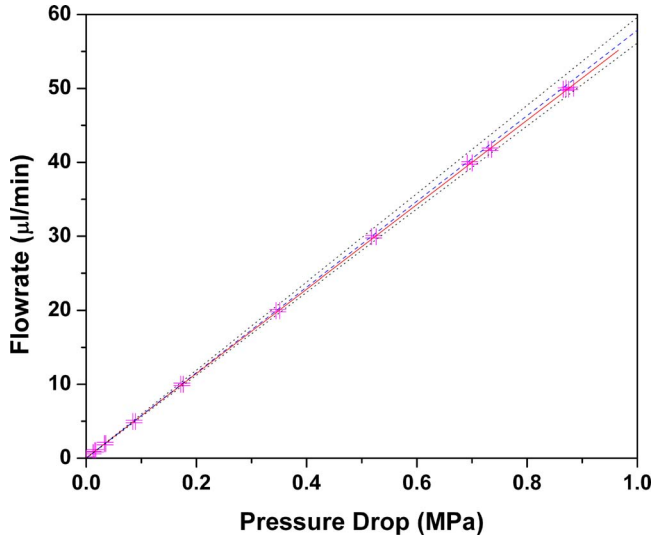

FIG. 5. (Color online) Measured flowrate vs imposed pressure drop for a test with ethanol flowing in a 5.02 μm deep channel. The solid line represents the linear fit of the experimental data, whose error bars are visible; the dashed line, the expected relation based on the measured dimensions. The two dotted lines represent the boundaries of the ±3% uncertainty level of this experiment. The experimental data fall within this interval.

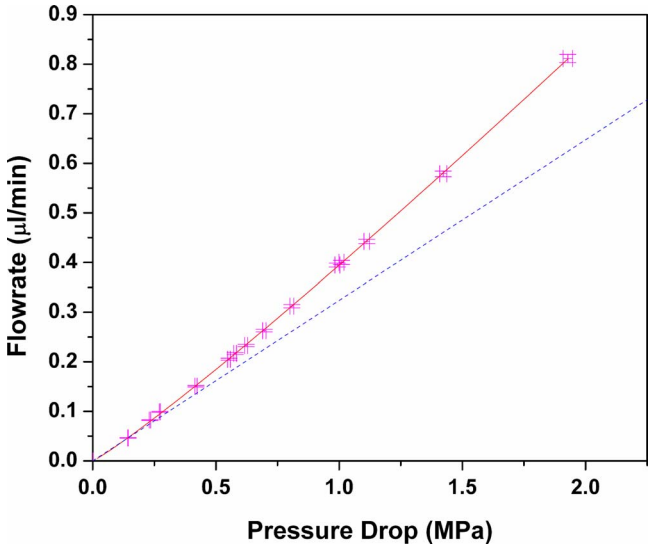

FIG. 7. (Color online) Measured flowrate vs imposed pressure drop for a test on isopropanol flowing in a smooth (R_a=0.5 nm) channel, 490 nm deep. The solid line represents the experimental fit of the data, whose error bars are visible; the dotted line, the expected relation based on the measured dimensions. The departure from linearity is apparent.

Tests performed with isopropanol and *n*-hexadecane on channels with depth ranging between 0.35 and 1.27 μm returned different results depending on the level of the wall surface roughness.

The experiments with rough submicron channels (isopropanol with H=0.81 μm, and *n*-hexadecane with H =0.53 μm; $R_a \sim 8.5$ nm in both cases) yielded, similarly to those with the 5 μm channels, a linear relation between $Q_{\text{experimental}}$ and Δp, with the difference between $Q_{\text{experimental}}$ and $Q_{\text{Poiseuille}}$ within experimental uncertainty (Fig. 6). The corresponding calculated slip length is therefore generally less than 5 nm and the slip velocity approximately zero. The negative values of slip length are explained with the experimental uncertainty. This finding is in agreement with numerical and experimental studies.[9,22,23]

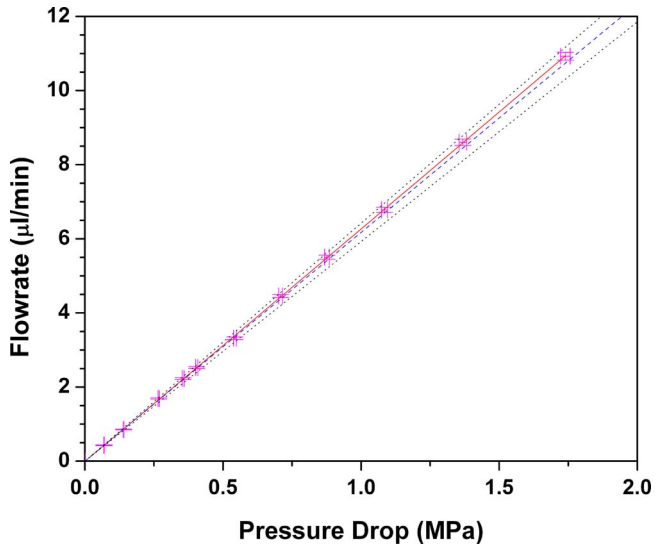

FIG. 6. (Color online) Flowrate vs pressure drop for a test on isopropanol flowing in a rough (R_a=8.5 nm) channel, 810 nm in height. The solid line represents the experimental fit of the data, whose error bars are visible; the dashed line, the expected relation based on the measured dimensions. The two dotted lines represent the ±4% uncertainty interval.

On the other hand, tests on smooth channels ($R_a \sim 0.5$ nm) show an increasingly pronounced departure from linearity in the relationship between $Q_{\text{experimental}}$ and Δp as the channel size decreases. With the only purpose of assessing the departure from linearity of the relation between the two quantities, the function $Q_{\text{experimental}}=C\cdot\Delta p^D$ was empirically chosen. The values D obtained from the least squares fits of the experimental data increase from slightly larger than 1.0 at 1.27 μm to ~1.2 at 0.35 μm. At the same time, the difference between $Q_{\text{experimental}}$ and $Q_{\text{Poiseuille}}$ becomes larger for smaller channels and increasingly exceeds the experimental uncertainty. Figure 7, showing the relation between experimental flowrate and pressure drop for isopropanol flowing in a 0.49 μm deep channel (D=1.1), is representative of the results obtained with smooth channels. The departure from the predicted values of $Q_{\text{Poiseuille}}$ translates into a slip length greater than zero, which is found to increase with the shear rate for both liquids. Hexadecane's slip length is several fold greater than isopropanol's, with a calculated value of around 120 nm at $\dot{\gamma}_w \sim 3\times 10^5$ s^{-1} for the former versus approximately 30 nm for the latter (Figs. 8 and 9). The respective slip velocities were around 40 and 10 mm/s at the same shear rate as above (Figs. 10 and 11). In both cases, the slip length and, consequently, the slip velocity vary with the shear rate. However, for a given fluid, the curves from different channels collapse onto each other, indicating that the slip length and slip velocity are independent of the channel height.

Assuming a $\beta=A\cdot\dot{\gamma}^B$ relationship based on the appearance of the data, the least squares fit of the two families of curves yields the values of the 0.42 and 0.52 for isopropanol

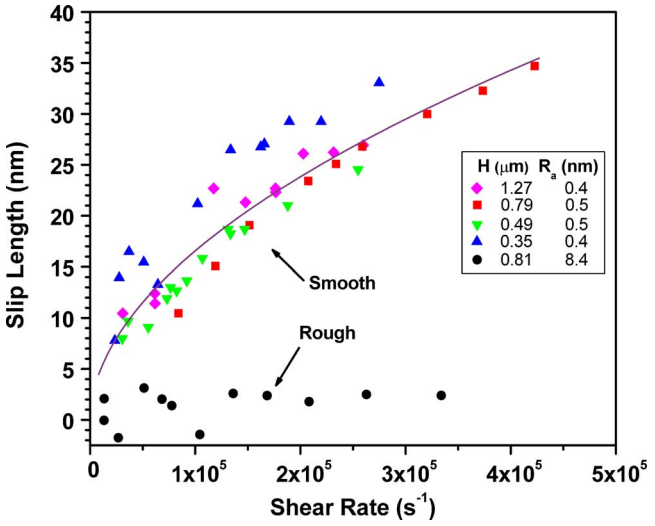

FIG. 8. (Color online) Calculated slip length vs shear rate for isopropanol, for different channel heights and levels of surface roughness. The solid line represents the experimental fit of the slip length for smooth channels.

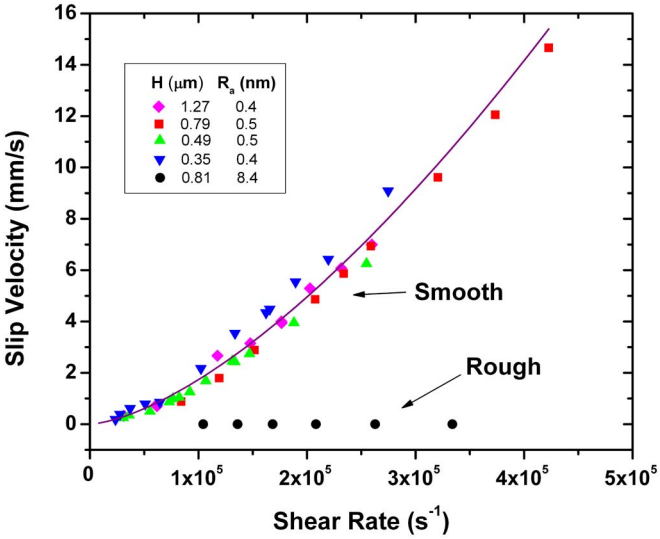

FIG. 10. (Color online) Calculated slip velocity vs shear rate for isopropanol, for different channel heights and levels of surface roughness. The solid line represents the experimental fit of the slip for smooth channels.

and hexadecane, respectively, for the B exponent, indicating a similar dependence between slip length and shear rate.

It is particularly interesting at this point to compare our data to that obtained by an experiment conducted under substantially similar conditions. Using micron-sized channels, Choi *et al.*[18] studied the slip length for water as a function of the shear rate and wall surface wettability (hydrophobic versus hydrophilic) on smooth channels. Slip was found to occur on both surfaces, with larger slip lengths on the hydrophobic boundary (nonwetting case). By comparison, we found that hexadecane on a hydrophilic surface (wetting case) displays a much greater slip length than water on a hydrophilic or hydrophobic surface (Fig. 12). More remarkably, the two studies present similar values of slip for water and isopropanol on a smooth hydrophilic surface.

Water and isopropanol molecules are similar in size (molecular radii of 2.82 and 4.85 Å, respectively), shape (approximately spherical), and permanent dipole moment (1.84 and 1.66 D, respectively). n-hexadecane, on the other hand, is a linear molecule several fold larger in length and is nonpolar. The picture that has emerged in the past decade from molecular dynamics simulations is that effective slip occurs in the first molecular layers of liquid in proximity of a solid surface. Slip is related to the level of both in-plane and out-of-plane ordering of the liquid molecules, which is ultimately due to two factors: (1) the strength of the liquid-solid interaction potential and (2) the degree of commensurability between liquid molecules and wall atoms, with the slip being greater for weaker interactions and lower levels of commensurability (Refs. 23 and 24 and references therein). The difference in slip between hexadecane, on one hand, and water and isopropanol, on the other, is therefore consistent with a different level of liquid-solid interaction due to the polarity of the liquid molecules. The surface slip also depends on the

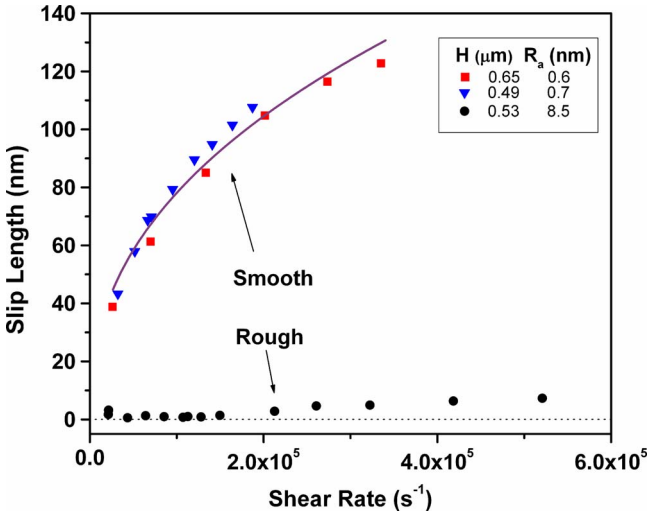

FIG. 9. (Color online) Calculated slip length vs shear rate for n-hexadecane, for different channel heights and levels of surface roughness. The solid line represents the experimental fit of the slip length for smooth channels.

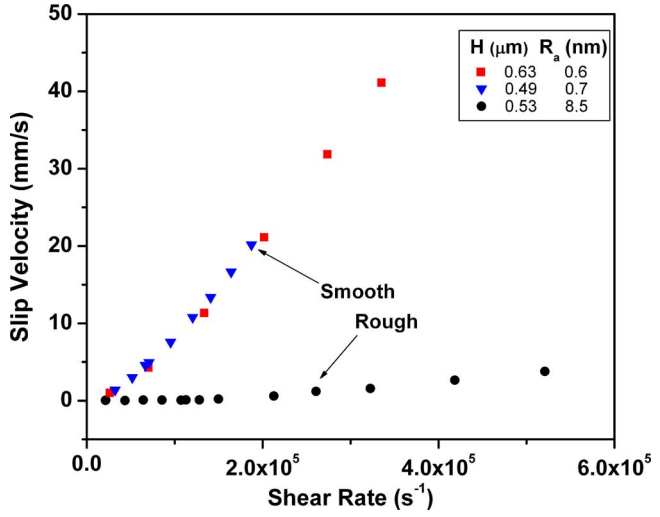

FIG. 11. (Color online) Calculated slip velocity vs shear rate for n-hexadecane, for different channel heights and levels of surface roughness.

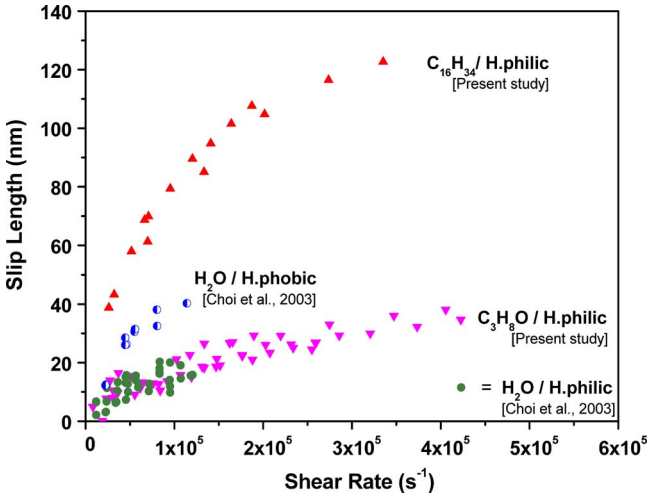

FIG. 12. (Color online) Slip length vs shear rate for water, isopropanol, and hexadecane on hydrophilic smooth surfaces, and water on a hydrophobic smooth surface.

surface property, hydrophobic or hydrophilic (or wetting versus nonwetting), when the same fluid was used.[18] Large slip was measured for hexadecane on a hydrophilic surface. In nanostructure-modified superhydrophobic channels, a very large slip length, 100–200 nm, is also observed for water.[25]

Finally, the fact that slip was not observed in the 5 μm deep smooth channels is explained by the fact that for larger channels the slip length is less affected by the channel size,[26] falling therefore beyond the sensitivity of the experimental apparatus.

VII. CONCLUSIONS

Experiments with Newtonian liquids such as isopropanol, *n*-hexadecane, water, ethanol, and toluene were conducted in microchannels with height of approximately 5 μm, and in channels with height between 350 nm and 1.27 μm with the first two liquids.

For channels with depth larger than 5 μm, none of the liquids tested showed a behavior different that predicted with the traditional no-slip boundary condition, while for smaller sizes the relation between flow rate and pressure drop in smooth channels consistently showed a departure from the predicted values. For rough channels the dependence of the flow rate on the pressure drop is linear and matches the predictions. For smooth channels below 1.27 μm in height, the flow rate depends on a power of the pressure drop which is greater than 1, and the measured flow rate is greater than the expected flow rate based on nonslip conditions. The slip effect becomes measurable in the range of 1 μm channel depth.

The relation between slip length and shear rate is independent of the channel height, while it does depend on the surface roughness and the type of liquid. For flow on rough surfaces, the slip length is found to be equal to zero, within experimental uncertainty. On smooth surfaces, *n*-hexadecane has shown surprisingly large slip lengths for flow on a hydrophilic (wetting) surface, with values as large as 120 nm at a shear rate of $\sim 3 \times 10^5$ s^{-1}, while slip lengths as large as 35 nm were measured for isopropanol. The amount of slip is found to be dependent on the polarity of the liquid molecules and is explained with the different energies of interaction between liquid molecules and substrate.

ACKNOWLEDGMENTS

This work is supported by NIH Metabolomics Project (Grant No. 1R33DK070328) and NIH Nanomedicine Roadmap Project (Grant No. PN2 EY018228).

[1] J. N. Israelachvili, *Intermolecular and Surface Forces*, 2nd ed. (Academic, London, UK, 1991).
[2] J. Koplik and J. R. Banavar, "Continuum deductions from molecular hydrodynamics," Annu. Rev. Fluid Mech. **27**, 257 (1995).
[3] C. Neto, D. R. Evans, E. Bonaccurso, H.-J. Butt, and V. S. J. Craig, "Boundary slip in Newtonian liquids: A review of experimental studies," Rep. Prog. Phys. **68**, 2859 (2005).
[4] E. Lauga, M. P. Brenner, and H. Stone, "Microfluidics: The no-slip boundary condition," *Handbook of Experimental Fluid Dynamics* (Springer, New York, 2005), Chap. 15.
[5] V. S. J. Craig, C. Neto, and D. R. M. Williams, "Shear-dependent boundary slip in an aqueous Newtonian liquid," Phys. Rev. Lett. **87**, 054504 (2001).
[6] Y. Zhu and S. Granick, "Limits of the hydrodynamic no-slip boundary condition," Phys. Rev. Lett. **88**, 106102 (2002).
[7] C. Cottin-Bizonne, A. Steinberger, B. Cross, O. Raccurt, and E. Charlaix, "Nanohydrodynamics: The intrinsic flow boundary condition on smooth surfaces," Langmuir **24**, 1165 (2008).
[8] C. Cottin-Bizonne, S. Jurine, J. Baudry, J. Crassous, F. Restagno, and E. Charlaix, "Nanorheology: An investigation of the boundary condition at hydrophobic and hydrophilic interfaces," Eur. Phys. J. E **9**, 47 (2002).
[9] R. Pit, H. Hervet, and L. Léger, "Direct experimental evidence of slip in hexadecane: Solid interfaces," Phys. Rev. Lett. **85**, 980 (2000).
[10] R. Pit, H. Hervet, and L. Léger, "Friction and slip of a simple liquid at a solid surface," Tribol. Lett. **7**, 147 (1999).
[11] P. Joseph and P. Tabeling, "Direct measurement of the apparent slip length," Phys. Rev. E **71**, 035303 (2005).
[12] T. Schmatko, H. Hervet, and L. Léger, "Friction and slip at simple fluid-solid interfaces: The roles of the molecular shape and the solid-liquid interaction," Phys. Rev. Lett. **94**, 244501 (2005).
[13] P. Huang, J. S. Guasto, and K. S. Breuer, "Direct measurement of slip velocities using three-dimensional total internal reflection velocimetry," J. Fluid Mech. **566**, 447 (2006).
[14] T. Schmatko, H. Hervet, and L. Léger, "Effect of nanometric-scale roughness on slip at the wall of simple fluids," Langmuir **22**, 6843 (2006).
[15] L. Zhu, D. Tretheway, L. Petzold, and C. Meinhart, "Simulation of fluid slip at 3D hydrophobic microchannel walls by the lattice Boltzmann method," J. Comput. Phys. **202**, 181 (2005).
[16] N. V. Churaev, V. Sobolev, and A. Somov, "Slippage of liquids over lyophobic solid surface," J. Colloid Interface Sci. **97**, 574 (1984).
[17] D. C. Tretheway and C. D. Meinhart, "Apparent fluid slip at hydrophobic microchannel walls," Phys. Fluids **14**, L9 (2002).
[18] C.-H. Choi, K. J. A. Westin, and K. S. Breuer, "Apparent slip flows in hydrophilic and hydrophobic microchannels," Phys. Fluids **15**, 2897 (2003).
[19] J. Pfahler, J. Harley, H. Bau, and J. N. Zemel, "Gas and liquid flow in small channels," in *Micromechanical Sensors, Actuators, and Systems* (ASME, New York, 1991), Vol. DSC-32.
[20] U. Ulmanella, "Molecular effects on the boundary condition in micro and nano fluidic channels," Ph.D. thesis, University of California, 2003.
[21] J. W. Benett and P. Krulevitch, "A flexible packaging and interconnect scheme for microfluidic systems," Proc. SPIE **3606**, 111 (1999).
[22] S. C. Yang and L. B. Fang, "Effect of surface roughness on slip flows in hydrophobic and hydrophilic microchannels by molecular dynamics simulation," Mol. Simul. **31**, 971 (2005).
[23] N. V. Priezjev, "Effect of surface roughness on rate-dependent slip in simple fluids," Phys. Rev. E **75**, 051605 (2007).
[24] N. V. Priezjev and S. M. Troian, "Influence of periodic wall roughness on

the slip behaviour at liquid/solid interfaces: Molecular-scale simulations versus continuum predictions," J. Fluid Mech. **554**, 25 (2006).
[25]C. H. Choi, U. Ulmanella, J. Kim, C. M. Ho, and C.-J. Kim, "Effective slip and friction reduction in nanograted superhydrophobic microchannels," Phys. Fluids **18**, 087105 (2006).
[26]J. Xu and Y. Li, "Boundary conditions at the solid-liquid surface over the multiscale channel size from nanometer to micron," Int. J. Heat Mass Transfer **50**, 2571 (2007).